ACS OMEGA

http://pubs.acs.org/journal/acsodf

Article

Functional Impact of a Cancer-Related Variant in Human Δ^1-Pyrroline-5-Carboxylate Reductase 1

Oseeyi I. Daudu, Kaylen R. Meeks, Lu Zhang, Javier Seravalli, John J. Tanner, and Donald F. Becker*

Cite This: *ACS Omega* 2023, 8, 3509−3519

Read Online

ACCESS | Metrics & More | Article Recommendations | Supporting Information

ABSTRACT: Pyrroline-5-carboxylate reductase (PYCR) is a proline biosynthetic enzyme that catalyzes the NAD(P)H-dependent reduction of Δ^1-pyrroline-5-carboxylate (P5C) to proline. Humans have three PYCR isoforms, with PYCR1 often upregulated in different types of cancers. Here, we studied the biochemical and structural properties of the Thr171Met variant of PYCR1, which is found in patients with malignant melanoma and lung adenocarcinoma. Although PYCR1 is strongly associated with cancer progression, characterization of a PYCR1 variant in cancer patients has not yet been reported. Thr171 is conserved in all three PYCR isozymes and is located near the P5C substrate binding site. We found that the amino acid replacement does not affect thermostability but has a profound effect on PYCR1 catalytic activity. The k_{cat} of the PYCR1 variant T171M is 100- to 200-fold lower than wild-type PYCR1 when P5C is the variable substrate, and 10- to 25-fold lower when NAD(P)H is varied. A 1.84 Å resolution X-ray crystal structure of T171M reveals that the Met side chain invades the P5C substrate binding site, suggesting that the catalytic defect is due to steric clash preventing P5C from achieving the optimal pose for hydride transfer from NAD(P)H. These results suggest that any impact on PYCR1 function associated with T171M in cancer does not derive from increased catalytic activity.

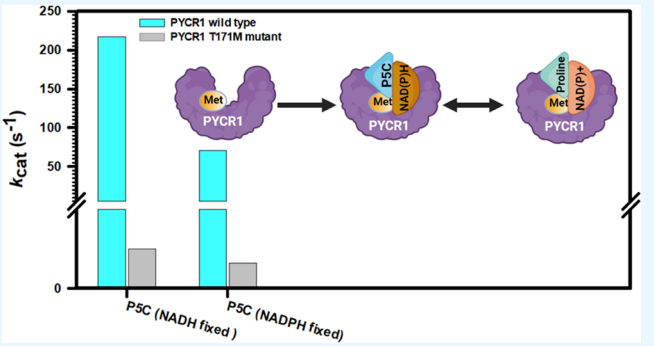

INTRODUCTION

Proline is unique among the standard 20 amino acids with its heterocyclic five-membered ring formed by its hydrophobic side chain and the amino nitrogen. Proline has important structural roles in proteins such as disrupting α-helix structures and stabilizing loops and turns. Collagen is highly abundant in proline, with a significant number of proline residues becoming post-translationally modified to hydroxyproline. Because collagen is a major structural component in bones, skin, cartilage, blood vessels, and connective tissues, one-third of the extracellular matrix, which is about 80% of the human body, is made up of proline.[1] Proline also regulates cellular processes such as apoptosis,[2] is utilized as a nutrient source under stress conditions,[3] and is important for redox homeostasis[4] and osmotic balance.[5]

Proline biosynthesis derives from glutamate and ornithine (Figure 1). Both pathways involve the metabolite Δ^1-pyrroline-5-carboxylate (P5C), which is reduced to proline by P5C reductase (PYCR in humans). There are three isoforms of PYCR, denoted PYCR1 (UniProt P32322), PYCR2 (UniProt Q96C36), and PYCR3 (a.k.a. PYCRL, UniProt Q53H96) (Figure 2). PYCR1 and PYCR2 are 84% identical in amino acid sequence and are primarily involved in proline biosynthesis from glutamate in the mitochondrion. PYCR3 is only 45% identical to PYCR1 and is localized in the cytosol.[6] It has been noted however that PYCR1 is active in high ornithine conditions[7] and can be recovered from the cytosol in small amounts.[8] Insufficient proline levels caused by deficiencies in PYCRs are linked to connective tissue disorders such as cutis laxa.[9]

PYCR1 has been implicated in the metabolic shift of cancer cells. A summary study done by D'Aniello et al. showed that the PYCR1 gene is linked to at least 22 different cancer types and is the most cancer-related gene of all of the proline metabolic enzymes.[10] A study done by Wang et al. showed that PYCR1 overexpression promotes proliferation and metastasis of lung cancer cells, and high expression of PYCR1 in patients with non-small-cell lung cancer correlates with poor prognosis.[8] Another study by Ye et al. on melanoma, a type of skin cancer, showed similar findings where an increase in PYCR1 expression correlated with increased melanoma cases.[11] PYCR1 has also been implicated in breast cancer,[12] melanoma,[7] multiple myeloma,[13] non-small lung cancer,[8] and

Received: December 6, 2022
Accepted: December 26, 2022
Published: January 10, 2023

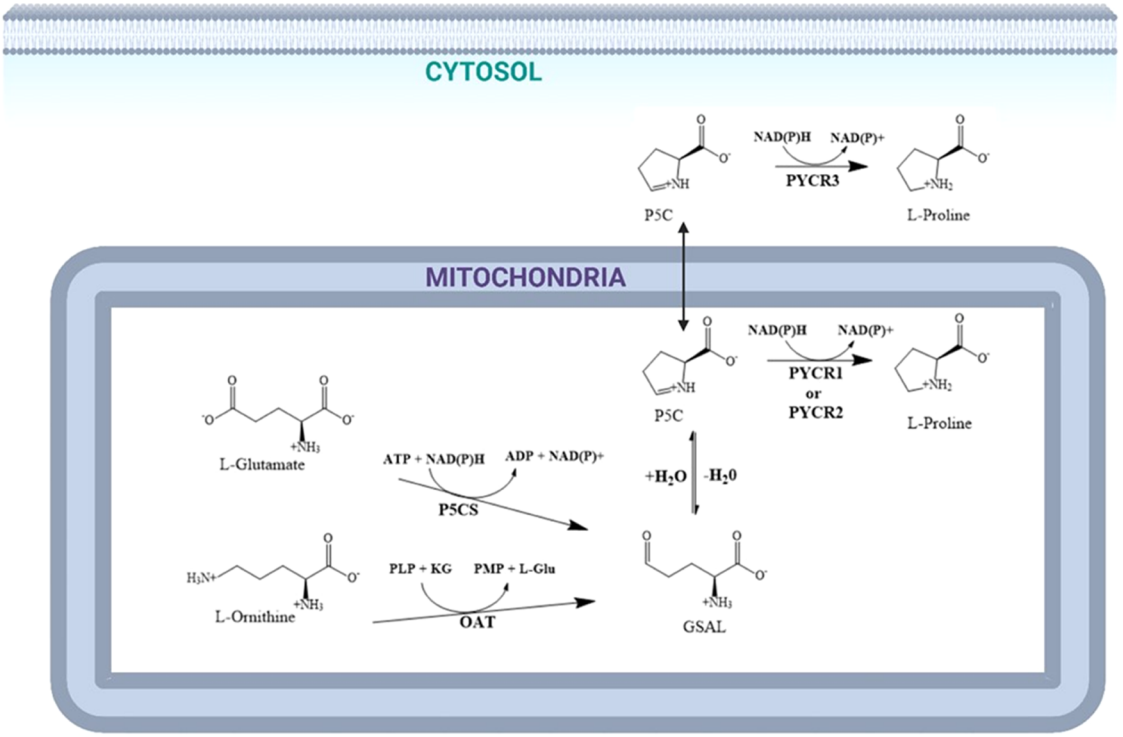

Figure 1. Enzymatic reactions of proline biosynthesis from ornithine in the cytosol (top) and from glutamate in mitochondria (bottom). Abbreviations used: OAT (ornithine-δ-aminotransferase), PLP (pyridoxal-5′-phosphate), PMP (pyridoxamine-5′-phosphate), α-KG (α-ketoglutarate), L-Glu (L-glutamate), P5CS (Δ^1-pyrroline-5-carboxylate synthase), ATP (adenosine triphosphate), ADP (adenosine diphosphate), nicotinamide adenine dinucleotide phosphate ($NADP^+$), reduced nicotinamide adenine dinucleotide phosphate (NADPH), PYCR1/2/3 (Δ^1-pyrroline-5-carboxylate reductases 1/2/3). Pathway illustration generated using ChemDraw and Biorender.com.

colorectal cancer,[14] for all of which a correlation between PYCR1 overexpression and metastatic growth has been shown.

Despite the number of studies that have been published on the role of PYCR1 in cancer, to our knowledge, there have been no reports on specific PYCR1 variants that are found in cancer patients. Herein, we report the biochemical and structural characterization of a PYCR1 missense variant found in cancer patients. Analysis of The Cancer Genome Atlas (TCGA) revealed a somatic mutation resulting in the Thr171Met variant of PYCR1 associated with skin and lung cancers. T171M was purified and characterized by steady-state kinetics and X-ray crystallography. The variant has a substantially lower catalytic activity. The structure suggests that this defect results from a steric clash between the side chain of Met171 and the substrate P5C.

RESULTS

Identification of a PYCR1 Variant Linked to Cancer. The Genomics Data Commons Data Portal was used to identify PYCR1 missense substitutions in samples from cancer patients.[15] We found 27 different variants in this initial screen that were associated with cancer. Of these, four variants in The Cancer Genome Atlas (TCGA) were selected based on being unique to PYCR1 and not in PYCR2 or PYCR3 (Supporting Information Table S1). The four PYCR1 variants found in TCGA were next cross-referenced with The Genome Aggregation Database (gnomAD)[16] to select for those not found in healthy individuals. After applying this filter, only one single-nucleotide variant resulting in a missense substitution in PYCR1 was identified that is specifically linked to cancer patients, Thr171Met (Supporting Information Table S1). We note that this missense replacement is denoted as T198M in databases that use UniProt P32322-3 as the reference sequence instead of the canonical PYCR1 sequence (UniProt P32322-1). The T171M PYCR1 variant is linked to lung and skin cancers.

Thr171 is located in the C-terminal domain of PYCR1, which is an α-helical domain involved in substrate binding and oligomerization.[17] The residue is part of an α-helix and begins a 7-residue stretch of amino acids that is identically conserved in all three PYCR isoforms (Figure 2). The helix to which Thr171 belongs forms one wall of the P5C/proline binding site.[17] The side chain of Thr171 hydrogen bonds to a water molecule that is conserved in PYCR1 structures (Figure 3). This water molecule bridges Thr171 to Arg119 and Gly98. Perhaps the most notable feature of Thr171 is that its methyl group contacts the pyrrolidine ring of P5C/proline at a distance of 3.6 Å (Figure 3). Thus, Thr171 appears to help orient the substrate P5C for hydride transfer from NADPH. The impact of substituting Thr171 with Met is predicted to be "moderate", "deleterious", or "probably damaging" by the programs VEP, SIFT, and PolyPhen, respectively.[18]

Thermostability of T171M. T171M was expressed in *Escherichia coli* and purified using procedures similar to wild-type PYCR1. We observed no significant differences in the expression and purification of T171M compared to wild-type PYCR1. Sodium dodecyl-sulfate polyacrylamide gel electrophoresis (SDS-PAGE) showed that the purity of T171M matched that of wild-type PYCR1 (Supporting Information Figure S1).

Many missense variants associated with inherited metabolic disorders affect protein stability,[20] therefore, we measured the

https://doi.org/10.1021/acsomega.2c07788
ACS Omega 2023, 8, 3509−3519

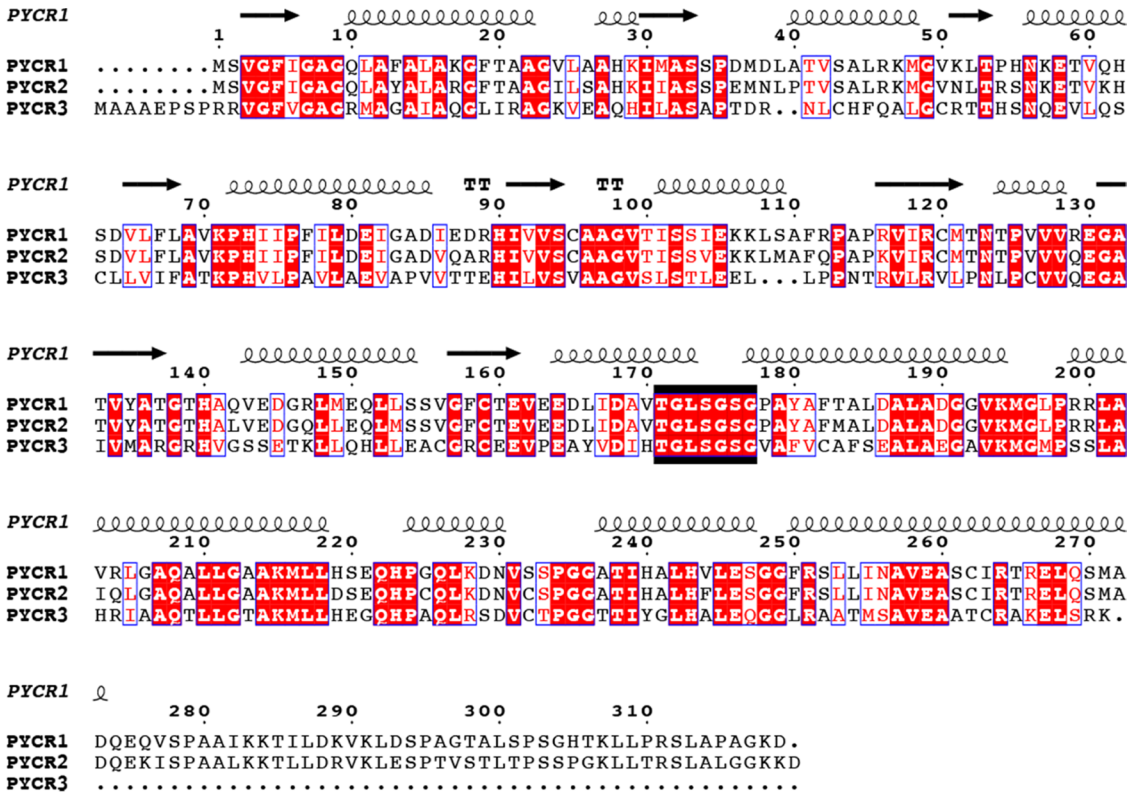

Figure 2. Multiple sequence alignment of human PYCR1 (UniProt P32322), PYCR2 (UniProt Q96C36), and PYCR3 (UniProt Q53H96). The secondary structure elements are from a structure of PYCR1 (PDB ID 5UAV). The black box indicates a conserved region containing Thr171. This figure was made with ESPript 3.0[18] from a multiple sequence alignment calculated in Clustal Omega.[19] This figure is adapted from Figure 3 of a previous publication on PYCR[6] (Bogner, A. N.; Stiers, K. M.; Tanner, J. J. Structure, biochemistry, and gene expression patterns of the proline biosynthetic enzyme pyrroline-5-carboxylate reductase (PYCR), an emerging cancer therapy target. Amino Acids 2021, 53 (12), 1817−1834. DOI: 10.1007/s00726-021-02999-5. PMID: 34003320; PMCID: PMC8599497).

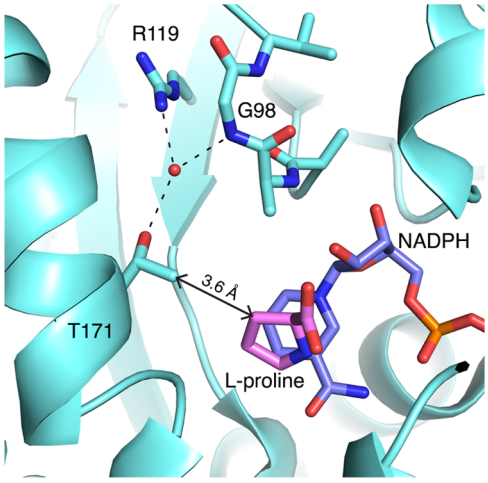

Figure 3. Structural context of Thr171 in PYCR1. Crystal structure of PYCR1 complexed with L-proline (pink) (PDB ID 5UAU). NADPH is superimposed from a structure of the PYCR1-NADPH complex (PDB ID 5UAT). Black dashes indicate hydrogen bonds. The closest contact between Thr171 and the product L-proline is 3.6 Å.

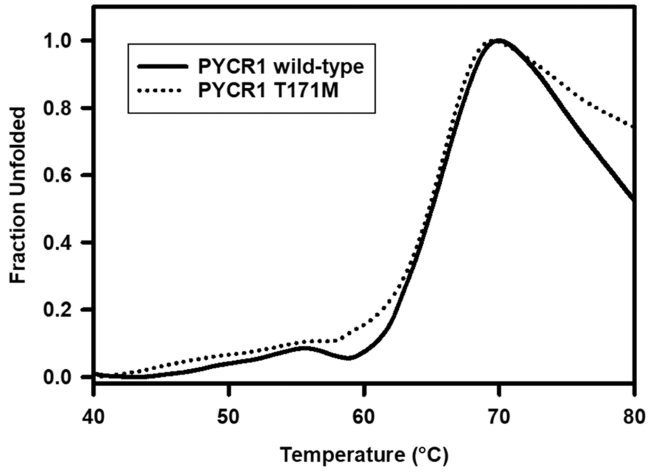

Figure 4. Fluorescence thermal shift analysis of PYCR1. Shown is the fraction of unfolded PYCR1 wild-type (straight line) and T171M (dotted lines) enzymes as a function of temperature. The melting point temperatures derived from this plot are 64.9 °C for PYCR1 wild-type and 64.8 °C for T171M. Plot was made using SigmaPlot 14.5.

thermostability of T171M using fluorescence thermal shift assays. The melting curves of PYCR1 wild-type and T171M are very similar and yielded nearly identical melting temperatures of nearly 65 °C, respectively (Figure 4). This suggests that the Met substitution does not substantially impact thermal stability.

T171M was also characterized by circular dichroism (CD). The CD spectrum of T171M is similar to that of wild-type PYCR1. The two spectra acquired at 37 °C are overlaid in Figure 5A. Both spectra exhibit prominent features at 200−220 nm. The correlation coefficient between the two spectra is 0.986 (Pearson moment product correlation), suggesting that

https://doi.org/10.1021/acsomega.2c07788
ACS Omega 2023, 8, 3509−3519

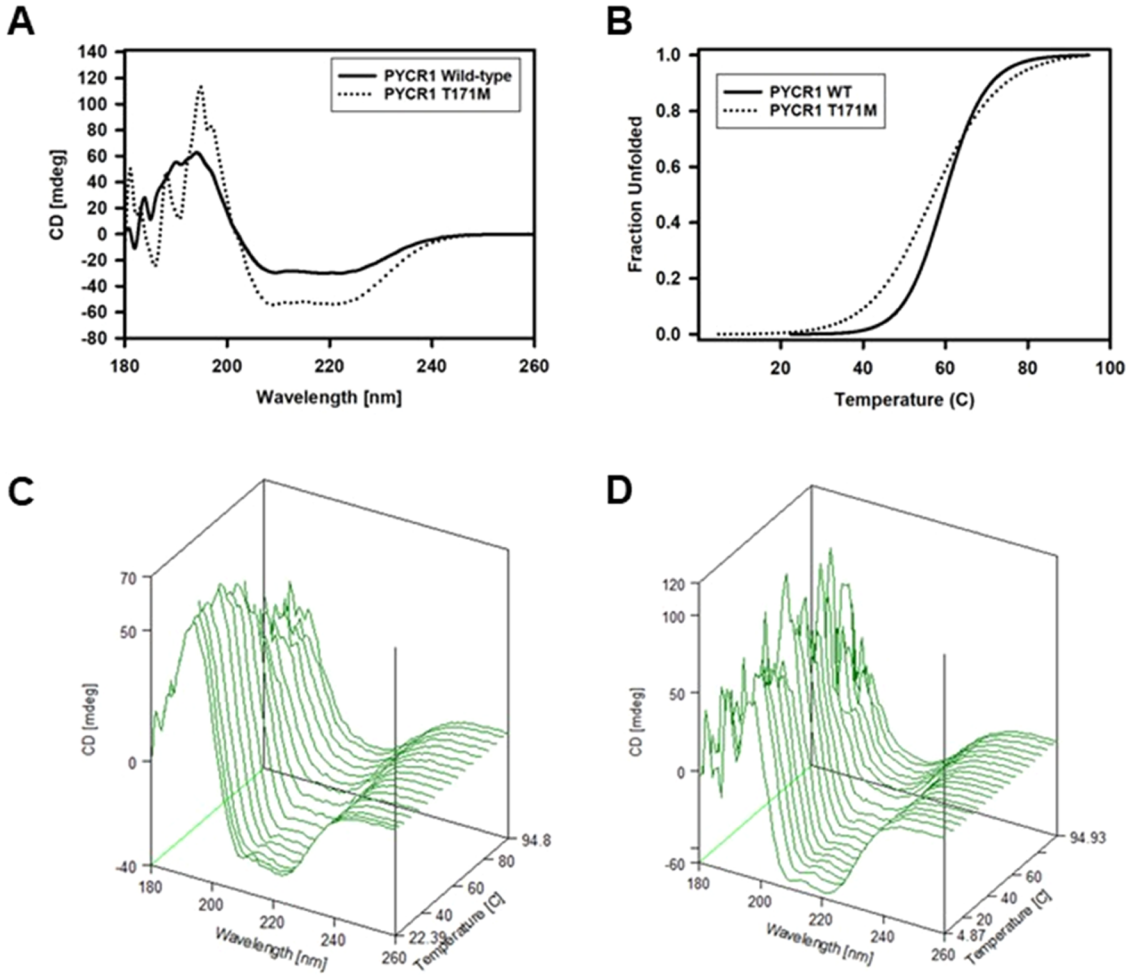

Figure 5. CD analysis of PYCR1 wild-type and T171M variant. (A) Overlay of the CD spectra of PYCR1 wild-type (solid line) and T171M (dotted lines) measured at 37 °C. (B) Thermal unfolding curves obtained by monitoring changes in CD at 222 nm for PYCR1 wild-type (solid line) and T171M (dotted line). Three-dimensional representation of CD thermal melt data for (C) PYCR1 wild-type and (D) T171M. Data in (A) and (B) were analyzed using SigmaPlot 14.5.

Table 1. Kinetic Parameters for PYCR1 Wild-Type and the T171M Variant[a]

varied substrate	fixed substrate	k_{cat} (s^{-1})	K_m (μM)	$k_{cat}/K_m \times 10^4$ (M^{-1} s^{-1})
		PYCR Wild-Type		
P5C	NADH	217 ± 21	677 ± 253	32 ± 12
P5C	NADPH	71 ± 3	373 ± 91	19 ± 5
NADH	P5C	85 ± 4	448 ± 54	19 ± 2
NADPH	P5C	25 ± 1	172 ± 25	15 ± 2
		PYCR T171M Variant		
P5C	NADH	1.0 ± 0.1	405 ± 134	0.3 ± 0.1
P5C	NAPDH	0.65 ± 0.02	114 ± 29	0.6 ± 0.2
NADH	P5C	3.5 ± 0.1	21.4 ± 5	16 ± 4
NADPH	P5C	2.6 ± 0.1	51 ± 12	5 ± 1

[a]Value ± std error are the apparent best-fit parameters from nonlinear least-squares fit of the data to the Henri−Michaelis−Menten equation using SigmaPlot 12.5. Data plotted as the (mean ± SD) of n = 3 technical replicates. Reported K_m values with P5C are the concentration of L-P5C, which is assumed to be half the concentration of the DL-P5C racemic mixture.

the Met replacement did not significantly impact the secondary structure of the enzyme. Thermal melting monitored by CD at 222 nm yielded melting temperatures of 59.4 and 57.3 °C for PYCR1 and T171M, respectively (Figure 5B−D). The CD analysis shows no significant difference in secondary structure between T171M and wild-type proteins, consistent with the mutation having minimal impact on thermostability.

Steady-State Kinetics. Kinetic assays were performed for PYCR1 wild-type and the T171M variant using DL-P5C as the variable substrate and NAD(P)H at a fixed saturating concentration of 0.5 mM. Plots of the initial rate as a function of DL-P5C concentration revealed that T171M has a substantially lower maximal velocity (Supporting Information Figure S2) than wild-type PCYR1. The k_{cat} for the T171M

https://doi.org/10.1021/acsomega.2c07788
ACS Omega 2023, 8, 3509−3519

PYCR1 variant is >200-fold lower with NADH, and >100-fold lower with NADPH relative to wild-type PYCR1 (Table 1). The estimated K_m values for P5C with the variant were slightly lower than that of wild-type PYCR1, resulting in catalytic efficiencies for the T171M variant that are 30- and 100-fold lower compared to wild-type using NADPH and NADH, respectively.

Kinetic assays were also performed with NAD(P)H as the variable substrate and keeping DL-P5C fixed. The initial rate data indicate a large defect in the maximal rate of T171M regardless of which reducing NAD(P)H substrate was used (Supporting Information Figure S3). The values for k_{cat} decreased by 25- and 10-fold relative to wild-type PYCR1 with NADH and NADPH, respectively (Table 1). The T171M variant reaches saturation with NAD(P)H at lower concentrations than wild-type PYCR1, resulting in lower apparent K_m values, particularly with NADH (Table 1). As a result, the apparent k_{cat}/K_m values for T171M are similar to wild-type PYCR1 when DL-P5C is held fixed (5 mM).

To further assess the functional impact of the Met replacement, assays were conducted using physiological concentrations of P5C (25 μM L-P5C)[21] and NAD(P)H substrates (30−40 μM).[22] Figure 6 shows that the activity of

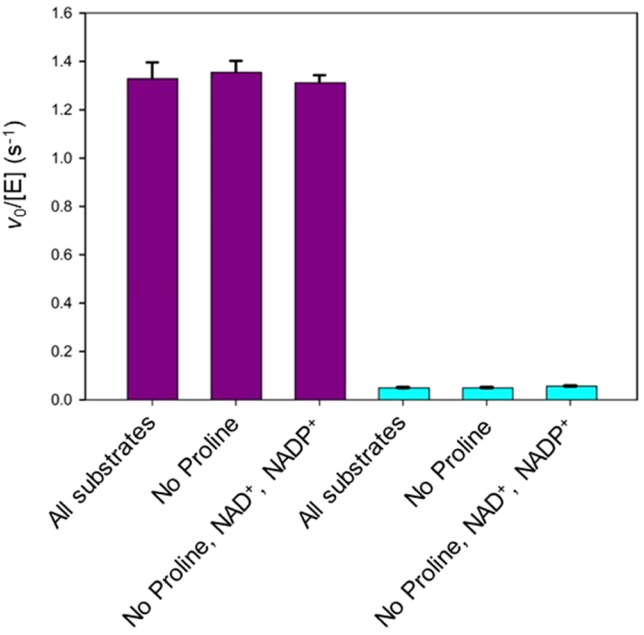

Figure 6. Activities of PYCR1 wild-type and T171M variant using physiological concentrations of substrates. Assays were performed in phosphate-buffered saline (PBS) (pH 7.5) with all substrates L-P5C (25 μM), NADH (30 μM), NAD^+ (200 μM), NADPH (40 μM), $NADP^+$ (4 μM), and L-proline (100 μM) (values are final concentrations in the assay). Assays were also conducted without L-proline and $NAD(P)^+$ as indicated. Shown are the mean velocity data (±standard deviation, n = 3 technical replicates) for PYCR1 wild-type (purple) and T171M variant (cyan). Data were analyzed using SigmaPlot 14.5.

the PYCR T171M variant (turnover number of 0.05 s^{-1}) is 26-fold lower than wild-type PCYR1 (1.3 s^{-1}) in assays with substrate concentrations that are relevant to mitochondria. Including $NAD(P)^+$ and L-proline in these assays did not influence the activity observed with the PYCR wild-type and variant enzymes. These results show that the PYCR1 T171M variant has a defective catalytic function under conditions that mimic substrate concentrations in the mitochondrion.

Crystal Structure of T171M. The structure of T171M complexed with NADH and was solved at 1.84 Å resolution. Purified PYCR1 T171M was co-crystallized in the presence of 2 mM NADH and 5 mM of the known PYCR1 inhibitor *N*-formyl-L-proline. Electron density for NADH is strong and indicates the typical binding pose of the cofactor bound to PYCR1 (Figure 7A). Although the inhibitor *N*-formyl-L-

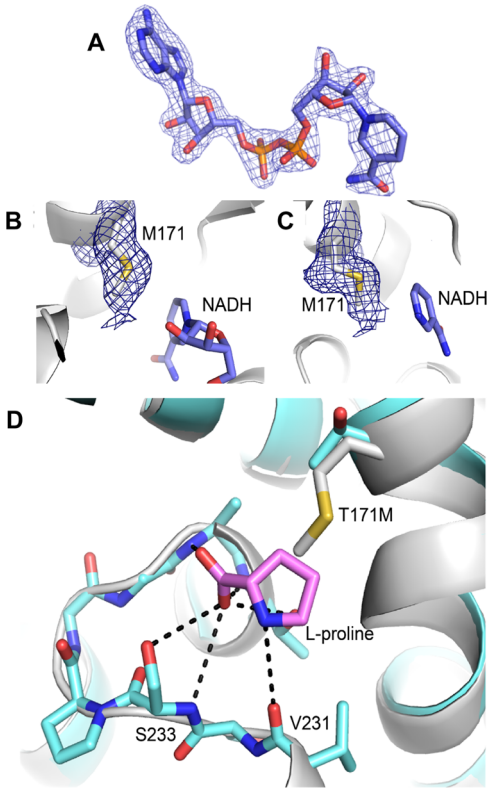

Figure 7. Crystal structure of the PYCR1 variant T171M. (A) Electron density for NADH (polder omit, 4σ). (B) Electron density for Met171 in chain D (polder omit, 4σ). (C) Electron density for Met171 in chain A (polder omit, 4σ). (D) Superposition of T171M (white) with PYCR1 complexed with L-proline (light blue with L-proline in pink, 5UAU). The dashed lines indicate enzyme−proline hydrogen bonds in 5UAU.

proline was also used in co-crystallization, clear electron density for the ligand was not observed. The maps did exhibit diffuse features that likely represent a sulfate ion bound in the active site with partial occupancy, which is common for PYCR1 crystals.

The Met substitution caused no discernible change to the tertiary or quaternary structure. The pairwise root-mean-square deviation (RMSD) between the chains of T171M and those of other human PYCR1 structures in the PDB spans the range of 0.17−1.01 Å. For reference, the pairwise RMSD between the chains of T171M is only 0.21−0.69 Å. Also, the enzyme crystallized as a pentamer-of-dimers decamer, as observed in all other PYCR1 structures. Evidence of a decamer for the PYCR1 T17M variant was also observed in solution by sedimentation velocity (Supporting Information Figure S4). Sedimentation velocity analysis indicated PYCR1 T171M exhibits both dimer and decamer species, consistent with previous sedimentation velocity analysis of wild-type PYCR1[17] and the observation of

https://doi.org/10.1021/acsomega.2c07788
ACS Omega 2023, 8, 3509−3519

a pentamer-of-dimers decamer in the crystal structures of both wild-type PYCR1 and T171M. Thus, the Met substitution does not appear to disrupt the oligomeric structure of the enzyme.

Electron density maps confirmed the mutation of Thr171 to Met. The shape of the density feature was somewhat variable among the five chains in the asymmetric unit. The density in chain A suggests a single conformation for the side chain of Met171 (Figure 7B). The electron density in the other chains indicated this conformation plus low occupancy of a second conformation; however, the density was considered insufficient to model the second confirmation (Figure 7C).

The mutation of Thr171 to Met is tolerated with minimal perturbation to the protein structure. The CB and CG atoms of Met171 are almost perfectly superimposed with the CB and methyl group of Thr171 (Figure 7D). The remaining two atoms of Met171 (SG and the methyl group) extend into the vacant space of the active site. In this conformation, Met171 invades the P5C/proline site. Superposition of the structures of T171M and the PYCR1-proline complex predicts a severe steric clash of less than 1 Å between the side chain of Met171 and P5C/proline (Figure 7D). The potential for clash likely inhibits the formation of the optimal Michaelis complex of the enzyme with P5C and NAD(P)H.

DISCUSSION

The *PYCR1* gene is commonly found upregulated across multiple types of cancers[6] with high PYCR1 levels associated with increased metastasis and poorer patient outcomes.[23] This observation has led to the hypothesis that the catalytic activity of PYCR1 is important in the metabolism of cancer cells. Consistent with this, several studies have reported that knockdown of *PYCR1* impairs cancer cell proliferation and tumorigenesis.[24] Additionally, small molecule inhibitors of PYCR1 have been shown to impair the spheroidal growth of MCF10A H-RAS^{V12} breast cancer cells[25] and proliferation of myelogenous erythroleukemic K562 and epithelial breast cancer MDA-MB-231 cell lines.[26] Recent therapeutic studies have shown that silencing of PYCR1 reduces the progression and proliferation of the cancer cells[27,28] and leads to the induction of apoptosis.[11] Increased apoptosis with loss of PYCR1 has also been reported in other diseases such as autosomal recessive cutis laxa.[9] PYCR1 disease-causing mutations were observed to increase susceptibility to apoptosis implicating PYCR1 in protecting mitochondria against oxidative stress.[9] Interestingly, mitochondrial respiratory chain activity was not impacted by the loss of PYCR1, suggesting that PYCR1 is not essential for respiratory chain function.[9]

With PYCR1 strongly implicated in cancer progression, we sought to determine the impact of PYCR1 variants that are identified uniquely in cancer patients. Analysis of the publicly available databases revealed the PYCR1 variant T171M is found in patients with certain skin and lung cancers. Interestingly, both types of cancers were shown previously to exhibit higher *PYCR1* expression.[6] Because PYCR1 promotes cancer cell growth and metastasis, we anticipated the T171M variant may exhibit enhanced catalytic activity. Unexpectedly, we found that PYCR1 T171M has substantially lower catalytic activity relative to wild-type PYCR1 with the greatest impact observed in catalytic efficiency with P5C (30- and 100-fold lower using NADPH and NADH, respectively).

The diminished activity observed with the T171M variant is not caused by significant changes in secondary structure or thermal stability. Circular dichroism and thermal stability measurements did not show significant differences between T171M and wild-type PYCR1. Insights into the effect of replacing Thr171 with Met were obtained by an X-ray crystal structure of the variant enzyme. Thr171 is close to the proline/P5C binding site in PYCR1. As shown in Figure 7D, the side chain of Met is likely to directly interfere with P5C binding, thus resulting in diminished catalytic activity. The lack of electron density for *N*-formyl-L-proline, which was included in co-crystallization and occupies the P5C/proline site of the wild-type enzyme (PDB ID 6XP0), in the crystal structure of T171M is consistent with the Met substitution interfering with substrate binding. Thr171 is conserved in human PYCR1, PYCR2, and PYCR3 suggesting that a Met replacement at the corresponding Thr residue would have the same effect in PYCR2 and PYCR3. Although the steric clash between Met171 and P5C is the simplest interpretation of the crystal structure, we acknowledge that the structure of the active site of T171M with P5C bound is unknown and could be different from the structure reported here. It is also possible that the mutation affected the flexibility of the active site, which could certainly influence the rate of catalytic turnover.

Why the PYCR1 Thr171Met variant is preferentially found in lung and skin cancer patients is not apparent. Splice variants of PYCR1, which are predicted to lack catalytic activity yet show strong association with cancer progression, present a similar conundrum.[6] The role of inactive PYCR1 splice variants in cancer is hypothesized to involve the loss of PYCR1 interactions with other proteins.[6] PYCR1 has been reported to interact with various proteins in different cancers such as Kindlin-2[29] in lung adenocarcinoma,[30] ORAOV1 in esophageal cancer,[31] and STAT3 in colorectal cancer.[32] PYCR1 has also been reported to interact with the Lon chaperon,[33] SIRT3 mitochondrial deacetylase,[34] ribonucleotide reductase small subunit B,[35] and other metabolic enzymes such as those involved in mitochondrial glycine, glutamate, and fatty acid metabolism.[36] Thus, the PYCR1 Thr171Met variant may exhibit different interactions with other proteins that influence cell signaling and ultimately disease progression.

Another consideration is the possibility of mixed alleles of PYCR1 wild-type and the T171M variant in the tumor which would enable some level of proline production. In addition, the PYCR2/3 isoforms could compensate for the significantly lower activity of the T171M variant. Accordingly, transcript levels of *PYCR2* and *PYCR3* are both increased in lung and skin cancer cell types. Thus, a compensatory mechanism caused by the PYCR1 T171M variant could lead to higher proline biosynthesis via PYCR2/3 which would support cancer cell growth. A related mechanism is the finding by Hollinshead et al.[37] that a mutation in isocitrate dehydrogenase 1 (Arg132His) results in upregulation of PYCR1 and proline biosynthesis in glioma tumor cells. It is proposed that PYCR1 provides an alternative source of NAD^+ that supports the TCA cycle when respiratory chain activity is low, thus ultimately promoting cancer cell progression.[37] PYCR1 was also shown recently to have a critical role in tumor cell growth by supporting redox homeostasis and the TCA cycle under hypoxic conditions.[27] Future work that examines whether the PYCR T171M variant reshapes proline metabolism in a way that favors cancer cell growth is needed to test this possibility.

https://doi.org/10.1021/acsomega.2c07788
ACS Omega 2023, 8, 3509−3519

CONCLUSIONS

The human PYCR1 variant T171M identified in cancer patients was found to have a significantly lower turnover number than wild-type PYCR1. Thus, cells harboring the T171M PYCR1 variant are anticipated to have lower levels of proline production. The large decrease in P5C reductase activity is likely due to the Met side chain directly interfering with binding of the P5C substrate. The ability to rewire metabolism is a hallmark of cancer cells and with a loss of PYCR1 activity in the T171M variant, it will be interesting to determine whether cells generate proline predominantly via PYCR2/3. How the T171M variant impacts interactions with proteins that influence cell signaling pathways is another important consideration. Last, finding the T171M PYCR1 variant in lung cancer and melanoma patients may contribute to the discovery of genes that increase susceptibility to these cancers. For example, melanoma is considered largely sporadic as only 10% of cases are known to be familiar with a large portion of these being due to a mutation in the gene encoding cyclin-dependent kinase 2A.[38] Identifying new gene variants linked to melanoma and exploring their role in carcinogenesis is essential for advancing our understanding of genetic risk factors.[39]

METHODS

Protein Purification. PYCR1 (UniProtKB P32322) was expressed from a pET-24b(+) plasmid containing a synthetic gene with codons optimized for expression in *E. coli*. As described previously, this construct encodes residues 1−300 of the full-length 319-residue protein plus an N-terminal hexahistidine tag and tobacco etch virus protease cleavage site.[17] Truncation of the C-terminus aids crystallization as previously described.[17,25] The plasmid encoding T171M was generated from this plasmid by GenScript.

The following procedures were used to generate both PYCR1 and T171M. Both constructs were expressed in *E. coli* BL21(DE3) and grown in terrific broth media containing 50 μg mL^{-1} kanamycin. A 20 mL starter culture was then used to inoculate two 1 L cultures. The culture was placed in a 37 °C shaker for approximately 6 h until the optical density at 600 nm (OD_{600}) was 0.8, at which point protein expression was induced by adding 0.2 mM IPTG to the culture for overnight induction at 18 °C. After overnight induction, the cells were incubated with 100 μg mL^{-1} chloramphenicol for 3 h at 18 °C as previously described.[40] The cells were then harvested by centrifugation at 5000 rpm for 20 min at 4 °C and stored at −80 °C.

The harvested cells were then resuspended in 50 mL of binding buffer (20 mM tris(hydroxymethyl)aminomethane, pH 7.4, 0.5 M NaCl, 5 mM imidazole, and 5% glycerol) containing five protease inhibitors (*ε*-amino-*N*-caproic acid, phenylmethylsulfonyl fluoride, *N*-tosyl-L-phenylalanyl chloromethyl ketone, *N*-*α*-*p*-tosyl-L-lysine chloromethyl ketone hydrochloride, and leupeptin) and 0.5% Triton X-100. The cells were broken on ice by sonication (Fisher Scientific 550 Sonic Dismembrator) for 5 min with 5 s on and 15 s off pulse settings, after which 0.2 g of *N*-octyl-*β*-D-glucopyranoside was added to the cell lysate solution and sonication was continued for one additional min (5 s on, 15 s off). After sonication, the cell lysate was stirred at 4 °C for 30 min and cell debris was removed by centrifugation at 16,000*g* for 30 min at 4 °C.

Table 2. X-ray Diffraction Data Collection and Refinement Statistics

beamline	APS 24-1D-E
space group	*C*2
unit cell parameters (Å, deg)	*a* = 110.60
	b = 179.93
	c = 88.30
	P = 107.01
wavelength (Å)	0.97918
resolution (Å)	91.18−1.87 (1.87−1.85)
observations[a]	977,058 (31394)
unique reflections[a]	140,673 (5414)
R_{merge} (I)[a]	0.128 (1.918)
R_{meas} (I)[a]	0.139 (2.098)
R_{pim} (I)[a]	0.052 (0.826)
mean I/σ[a]	11.6 (0.7)
$CC_{1/2}$[a]	0.998 (0.435)
completeness (%)[a]	98.5 (76.7)
multiplicity[a]	6.9 (5.8)
no. of protein residues	1389
No. of Atoms	
protein	9976
NADH	220
SO_4	40
water	425
R_{cryst}[a]	0.188 (0.382)
R_{free}[a,b]	0.217 (0.388)
RMSD bonds (Å)	0.007
RMSD angle (deg)	0.856
Ramachandran Plot[c]	
favored (%)	97.97
outliers (%)	0.00
clashscore (PR)[c]	2.36 (99)
MolProbity score (PR)[c]	1.08 (100)
Average B (Å^2)	
protein	38.9
NADH	44.7
water	40.1
SO_4	52.5
PDB ID	8DKG

[a]Values for the outer resolution shell of data are given in parentheses. [b]5% test set. [c]From MolProbity. The percentile ranks (PR) for Clashscore and MolProbity score are given in parentheses.

PYCR1 wild-type and T171M variant proteins were purified by immobilized metal affinity chromatography using Nickel-Nitriloacetic acid (Ni-NTA) resin. The Ni-NTA column was loaded with the supernatant and placed in a 4 °C cold room overnight, the supernatant was then run through the column twice. The resin was next washed with 10 column volumes of the washing buffer (binding buffer + 30 mM imidazole), followed by 10 column volumes of binding buffer. The target protein was eluted with 5 volumes of elution buffer (binding buffer + 500 mM imidazole). The elution fraction was put into 1 L of dialysis buffer (50 mM Tris-HCl pH 8.0, 25 mM NaCl, 0.5 mM EDTA, and 10% glycerol) for 4 h, and then the sample was transferred to a fresh 1 L dialysis buffer overnight. The histidine tag was not removed. Proteins were concentrated using an ultrafiltration stirred cell (Model 8050, Amicon EMD Millipore-Sigma), with a 5 kDa PLCC low bind 44.5 mm diameter ultracentrifugation disc (EMD Millipore-Sigma) at 4

https://doi.org/10.1021/acsomega.2c07788
ACS Omega 2023, 8, 3509−3519

°C. The enzyme concentration was determined using the Pierce 660 nm Protein Assay Reagent (Thermo-Fisher Scientific Pierce Biotech) using bovine serum albumin as the standard. The wild-type and T171M proteins were flash-frozen in liquid nitrogen at 1.2 and 0.8 mg mL^{-1}, respectively, and stored at −80 °C.

Kinetic Measurements. Steady-state kinetic analysis was performed using DL-P5C and NAD(P)H as the substrates and monitoring the loss of NAD(P)H at 340 nm (ε_{340} = 6.22 mM^{-1} cm^{-1}) and 380 nm (ε_{380} = 1.314 mM^{-1} cm^{-1}) with a UV−vis spectrophotometer (Cary-50, Varian-Agilent). Assays were performed in spectrophotometric cuvettes (optical path length = 1cm) at 37 °C in 0.1 M Tris-HCl (pH 7.5) buffer containing 1 mM EDTA and 0.01% Brij-35 detergent (Santa Cruz Biotechnology), varying concentrations of DL-P5C and NAD(P)H, and 0.05 μM PYCR1 wild-type or 0.5 μM PYCR1 T171M for a total reaction volume of 600 μL. Initial assays indicated that T171M has a defect in catalytic activity, thus the kinetic constants for the T171M variant were determined using a 10-fold higher enzyme concentration than that of wild-type PYCR1.

DL-P5C used was synthesized as described previously[40] according to the protocol by Williams et al.[41] and was freshly neutralized with 6 M NaOH to pH 7 immediately prior to the assays. In assays with DL-P5C as the variable substrate, NAD(P)H concentration was held fixed at 500 μM, whereas in assays with NAD(P)H as the variable substrate, DL-P5C concentration was kept fixed at 5 mM. A mixture of the Tris-HCl buffer, NAD(P)H, and DL-P5C was preheated at 37 °C for 5 min prior to each reaction. Reactions were initiated by adding the PYCR1 enzyme, and the reactions were monitored for 2 min with all assays performed in triplicate.

Absorbance changes over the first min of the reaction were used to calculate the initial velocity (v_0, μM s^{-1}) using extinction coefficients of 1.314 mM^{-1} cm^{-1} at 380 nm for NADPH and 6.220 mM^{-1} cm^{-1} at 340 nm for NADH.[7] The initial velocity data were fitted to the Michaelis−Menten equation using SigmaPlot v12.5 (Systat Software Inc.) to obtain the steady-state kinetic parameters.

Assays were also conducted under conditions designed to mimic physiological substrate concentrations, as that reported previously for P5C reductase from *Saccharomyces cerevisiae*.[42] These assays were performed at 23 °C in phosphate-buffered saline (PBS) solution (10 mM Na_2HPO_4, 1.8 mM KH_2PO_4, 137 mM NaCl, 2.7 mM KCl, pH 7.5) containing DL-P5C (50 μM)[21] and different combinations of NADH (30 μM),[43] NAD^+ (200 μM),[44] NADPH (40 μM),[45] $NADP^+$ (4 μM),[22] and L-proline (100 μM) in a total reaction volume of 1 mL. Reactions were initiated by adding enzyme (0.5 μM final concentration for PYCR1 wild-type and T171M), and initial velocities (v_0, μM s^{-1}) were determined by monitoring the absorbance decrease at 340 nm.

Thermal Shift Assays. The enzyme was dialyzed into 100 mM potassium phosphate buffer (pH 7.0) prior to analysis. For melting point analysis, 6 μM enzyme (final concentration after mixing) was added to a PCR tube containing 5 μL of 25× SYPRO orange dye (Bio-Rad) and then balanced with 100 mM potassium phosphate buffer (pH 7.0) to make a final 50 μL total reaction volume. The tubes were covered with aluminum foil and then placed on a shaker at 4 °C for 2 h. Thermal denaturation assays were performed using Bio-Rad CFX Connect real-time PCR detection system, with a temperature range of 20−90 °C with 0.2 °C intervals per 15 s. Data were analyzed using SigmaPlot 14.5 (Systat Software).

Circular Dichroism. The enzymes were dialyzed into a 10 mM sodium phosphate buffer (pH 8.0) prior to analysis. For CD thermal melt analysis, 24.2 μM wild-type PYCR1 was heated from 22 to 95 °C in 5 °C intervals. Similarly, 20.6 μM T171M was heated from 5 to 95 °C with 5 °C intervals. The wavelength range monitored was 180−260 nm. The melting point analysis was done at 222 nm for both enzymes by fitting the data (SigmaPlot 14.5) to the following equations:

$$\delta = \alpha^*(\Delta U - \Delta F) + \Delta F$$

$$\alpha = \exp(-\Delta G/RT)/(1 + \exp(-\Delta G/RT))$$

$$\Delta G = \Delta H^*(1 - T/T_m)$$

$T = x + 273.15$ where δ is the (y-axis) signal, ΔG is the Gibbs free energy, ΔH is the enthalpy change and T_m is the melting point.

Sedimentation Velocity Analysis. The oligomeric structure of the PYCR1 T171M variant was characterized by sedimentation velocity ultracentrifugation. Sedimentation velocity experiments were performed at 20 °C using an Optima XL-I analytical ultracentrifuge (Beckman Coulter, Inc.) equipped with an eight-hole An50Ti rotor. The PYCR1 T171M variant was analyzed at 4.3 mg mL^{-1} in 50 mM Tris (pH 8) containing 150 mM NaCl. The protein sample (400 μL) and buffer control were loaded into their respective compartments of a double-sector cell. After incubation of 2 h at 20 °C, the protein sample was centrifuged at 40,000 rpm with a total of 200 absorbance scans at 290 nm recorded at 2 min intervals. The data from scans 20−200 were analyzed assuming a partial specific volume of 0.73 mL g^{-1} with SEDFIT version 10.58d[46] using the continuous $c(s)$ distribution model to generate the apparent $c(s)$ distribution. The frictional ratio value was fixed at 1.7 after initially being set at 1.94 as reported previously for wild-type PYCR1.[17]

X-ray Crystal Structure Determination of T171M. Following the procedures used for the wild-type enzyme,[17,25] T171M (10 mg mL^{-1}) was co-crystallized with NADH (2 mM) and the inhibitor *N*-formyl-L-proline (5 mM). Crystals were grown in sitting drops at 20 °C using a reservoir solution of 0.36 M Li_2SO_4, 0.1 M 4-(2-hydroxyethyl)-1-piperazineethanesulfonic acid (HEPES) pH 7.5, and 20% (w/v) PEG 3350. Sitting drops were formed by combining 2 μL of reservoir solution with 2 μL of protein−ligand solution. Drops were seed streaked with wild-type PYCR1 microcrystals. Crystals were cryo-protected with 20% PEG 200 and flash-cooled in liquid nitrogen. Additional NADH and *N*-formyl-L-proline were not included in the cryo-buffer.

X-ray diffraction data were collected at Advanced Photon Source beamline 24-ID-E (Eiger-16M detector). The data were processed with XDS[47] and AIMLESS.[48] The space group is *C*2, and the asymmetric unit contains five chains arranged as one-half of a pentamer-of-dimers decamer. We note this is a PYCR1 crystal form that we have used previously (PDB ID 6XP3).[25] The starting model used for refinement was derived from a deposited structure of PYCR1 (PDB ID 6XP3). PHENIX and Coot[49] were used for iterative model building and crystallographic refinement.[50] The structure was validated using the MolProbity,[51] the wwPDB validation service,[52] and polder omit maps.[53] Data processing and refinement statistics are listed in Table 2. The coordinates and structure factor amplitudes have been deposited in the PDB under the accession code 8DKG.

https://doi.org/10.1021/acsomega.2c07788
ACS Omega 2023, 8, 3509−3519

■ ASSOCIATED CONTENT

Supporting Information

The Supporting Information is available free of charge at https://pubs.acs.org/doi/10.1021/acsomega.2c07788.

PYCR1 variants identified in cancer patients (Table S1); SDS-PAGE of Purified PYCR1 proteins (Figure S1); Michaelis−Menten plots of PYCR1 with varying L-P5C (Figure S2); Michaelis−Menten analysis of PYCR1 with varying NADH and NADPH (Figure S3); and sedimentation velocity analysis of PYCR1 T171M (Figure S4) (PDF)

Accession Codes

The coordinates and structure factor amplitudes have been deposited in the PDB with the accession code 8DKG.

■ AUTHOR INFORMATION

Corresponding Author

Donald F. Becker − *Department of Biochemistry, Redox Biology Center, University of Nebraska, Lincoln, Nebraska 68588, United States;* orcid.org/0000-0002-1350-7201; Email: dbecker3@unl.edu

Authors

Oseeyi I. Daudu − *Department of Biochemistry, Redox Biology Center, University of Nebraska, Lincoln, Nebraska 68588, United States*

Kaylen R. Meeks − *Department of Biochemistry, University of Missouri, Columbia, Missouri 65211, United States;* orcid.org/0000-0001-9024-6255

Lu Zhang − *Department of Biochemistry, Redox Biology Center, University of Nebraska, Lincoln, Nebraska 68588, United States*

Javier Seravalli − *Department of Biochemistry, Redox Biology Center, University of Nebraska, Lincoln, Nebraska 68588, United States*

John J. Tanner − *Department of Biochemistry, University of Missouri, Columbia, Missouri 65211, United States; Department of Chemistry, University of Missouri, Columbia, Missouri 65211, United States;* orcid.org/0000-0001-8314-113X

Complete contact information is available at: https://pubs.acs.org/10.1021/acsomega.2c07788

Author Contributions

All authors helped with the design of experiments. O.I.D. conducted the purification and experiments with PYCR1 wild-type and the T171M variant. K.R.M. performed the crystallography experiments. J.S. performed the circular dichroism experiments. All authors contributed to data analysis and interpretation and to the writing of the manuscript and have approved the final version of the manuscript

Notes

The authors declare no competing financial interest.

■ ACKNOWLEDGMENTS

Research reported in this publication was supported in part by the National Institute of General Medical Sciences of the National Institutes of Health under award number R01GM13264. The results shown here are partly based upon data generated by the TCGA Research Network: https://www.cancer.gov/tcga. The Genome Aggregation Database (gnomAD) was accessed on 3/25/22 from https://registry.opendata.aws/broad-gnomad. The authors thank Jonathan Schuermann for help with X-ray diffraction data collection and processing, and Sagar Patel for his input in the experimental setup on the kinetics and thermal stability assays. This work is based upon research conducted at the Northeastern Collaborative Access Team beamlines, which are funded by the National Institute of General Medical Sciences from the National Institutes of Health (P30 GM124165). The Eiger 16M detector on the 24-ID-E beamline is funded by an NIH-ORIP HEI grant (S10OD021527). This research used resources of the Advanced Photon Source, a U.S. Department of Energy (DOE) Office of Science User Facility operated for the DOE Office of Science by Argonne National Laboratory under Contract No. DE-AC02-06CH11357.

■ ABBREVIATIONS

CD, circular dichroism; gnomAD, The Genome Aggregation Database; NADPH, nicotinamide adenine dinucleotide phosphate; $NADP^+$, nicotinamide adenine dinucleotide phosphate; P5C, Δ^1-pyrroline-5-carboxylate; PBS, phosphate-buffered saline; PYCR1, P5C reductase 1; TCGA, The Cancer Genome Atlas

■ REFERENCES

(1) Hu, S.; He, W.; Wu, G. Hydroxyproline in animal metabolism, nutrition, and cell signaling. *Amino Acids* **2022**, *54*, 513−528.

(2) Phang, J. M. Proline Metabolism in Cell Regulation and Cancer Biology: Recent Advances and Hypotheses. *Antioxid. Redox Signaling* **2019**, *30*, 635−649.

(3) Phang, J. M.; Donald, S. P.; Pandhare, J.; Liu, Y. The metabolism of proline, a stress substrate, modulates carcinogenic pathways. *Amino Acids* **2008**, *35*, 681−690.

(4) Tanner, J. J.; Fendt, S. M.; Becker, D. F. The Proline Cycle As a Potential Cancer Therapy Target. *Biochemistry* **2018**, *57*, 3433−3444.

(5) Kazama, D.; Kurusu, T.; Mitsuda, N.; Ohme-Takagi, M.; Tada, Y. Involvement of elevated proline accumulation in enhanced osmotic stress tolerance in Arabidopsis conferred by chimeric repressor gene silencing technology. *Plant Signaling Behav.* **2014**, *9*, No. e28211.

(6) Bogner, A. N.; Stiers, K. M.; Tanner, J. J. Structure, biochemistry, and gene expression patterns of the proline biosynthetic enzyme pyrroline-5-carboxylate reductase (PYCR), an emerging cancer therapy target. *Amino Acids* **2021**, *53*, 1817−1834.

(7) De Ingeniis, J.; Ratnikov, B.; Richardson, A. D.; Scott, D. A.; Aza-Blanc, P.; De, S. K.; Kazanov, M.; Pellecchia, M.; Ronai, Z.; Osterman, A. L.; Smith, J. W. Functional specialization in proline biosynthesis of melanoma. *PLoS One* **2012**, *7*, No. e45190.

(8) Wang, D.; Wang, L.; Zhang, Y.; Yan, Z.; Liu, L.; Chen, G. PYCR1 promotes the progression of non-small-cell lung cancer under the negative regulation of miR-488. *Biomed. Pharmacother.* **2019**, *111*, 588−595.

(9) Reversade, B.; Escande-Beillard, N.; Dimopoulou, A.; Fischer, B.; Chng, S. C.; Li, Y.; Shboul, M.; Tham, P. Y.; Kayserili, H.; Al-Gazali, L.; et al. Mutations in PYCR1 cause cutis laxa with progeroid features. *Nat. Genet.* **2009**, *41*, 1016−1021.

(10) D'Aniello, C.; Patriarca, E. J.; Phang, J. M.; Minchiotti, G. Proline Metabolism in Tumor Growth and Metastatic Progression. *Front. Oncol.* **2020**, *10*, 776.

(11) Ye, Y.; Wu, Y.; Wang, J. Pyrroline-5-carboxylate reductase 1 promotes cell proliferation via inhibiting apoptosis in human malignant melanoma. *Cancer Manage. Res.* **2018**, *10*, 6399−6407.

(12) Ding, J.; Kuo, M. L.; Su, L.; Xue, L.; Luh, F.; Zhang, H.; Wang, J.; Lin, T. G.; Zhang, K.; Chu, P.; et al. Human mitochondrial pyrroline-5-carboxylate reductase 1 promotes invasiveness and impacts survival in breast cancers. *Carcinogenesis* **2017**, *38*, 519−531.

(13) Oudaert, I.; Satilmis, H.; Vlummens, P.; De Brouwer, W.; Maes, A.; Hose, D.; De Bruyne, E.; Ghesquiere, B.; Vanderkerken, K.; De Veirman, K.; Menu, E. Pyrroline-5-Carboxylate Reductase 1: a novel target for sensitizing multiple myeloma cells to bortezomib by inhibition of PRAS40-mediated protein synthesis. *J. Exp. Clin. Cancer Res.* **2022**, *41*, 45.
(14) Alaqbi, S. S.; Burke, L.; Guterman, I.; Green, C.; West, K.; Palacios-Gallego, R.; Cai, H.; Alexandrou, C.; Myint, N. N. M.; Parrott, E.; et al. Increased mitochondrial proline metabolism sustains proliferation and survival of colorectal cancer cells. *PLoS One* **2022**, *17*, No. e0262364.
(15) Grossman, R. L.; Heath, A. P.; Ferretti, V.; Varmus, H. E.; Lowy, D. R.; Kibbe, W. A.; Staudt, L. M. Toward a Shared Vision for Cancer Genomic Data. *N. Engl. J. Med.* **2016**, *375*, 1109−1112.
(16) Karczewski, K. J.; Francioli, L. C.; Tiao, G.; Cummings, B. B.; Alfoldi, J.; Wang, Q.; Collins, R. L.; Laricchia, K. M.; Ganna, A.; Birnbaum, D. P.; et al. The mutational constraint spectrum quantified from variation in 141,456 humans. *Nature* **2020**, *581*, 434−443.
(17) Christensen, E. M.; Patel, S. M.; Korasick, D. A.; Campbell, A. C.; Krause, K. L.; Becker, D. F.; Tanner, J. J. Resolving the cofactor-binding site in the proline biosynthetic enzyme human pyrroline-5-carboxylate reductase 1. *J. Biol. Chem.* **2017**, *292*, 7233−7243.
(18) Robert, X.; Gouet, P. Deciphering key features in protein structures with the new ENDscript server. *Nucleic Acids Res.* **2014**, *42*, W320−W324.
(19) Sievers, F.; Wilm, A.; Dineen, D.; Gibson, T. J.; Karplus, K.; Li, W.; Lopez, R.; McWilliam, H.; Remmert, M.; Soding, J.; et al. Fast, scalable generation of high-quality protein multiple sequence alignments using Clustal Omega. *Mol. Syst. Biol.* **2011**, *7*, 539.
(20) Shi, Z.; Sellers, J.; Moult, J. Protein stability and in vivo concentration of missense mutations in phenylalanine hydroxylase. *Proteins* **2012**, *80*, 61−70.
(21) Merrill, M. J.; Yeh, G. C.; Phang, J. M. Purified human erythrocyte pyrroline-5-carboxylate reductase. Preferential oxidation of NADPH. *J. Biol. Chem.* **1989**, *264*, 9352−9358.
(22) Williamson, D. H.; Lund, P.; Krebs, H. A. The redox state of free nicotinamide-adenine dinucleotide in the cytoplasm and mitochondria of rat liver. *Biochem. J.* **1967**, *103*, 514−527.
(23) Li, Y.; Xu, J.; Bao, P.; Wei, Z.; Pan, L.; Zhou, J.; Wang, W. Survival and clinicopathological significance of PYCR1 expression in cancer: A meta-analysis. *Front. Oncol.* **2022**, *12*, No. 985613.
(24) Wang, Q. L.; Liu, L. PYCR1 is Associated with Papillary Renal Cell Carcinoma Progression. *Open Med.* **2019**, *14*, 586−592.
(25) Christensen, E. M.; Bogner, A. N.; Vandekeere, A.; Tam, G. S.; Patel, S. M.; Becker, D. F.; Fendt, S. M.; Tanner, J. J. In crystallo screening for proline analog inhibitors of the proline cycle enzyme PYCR1. *J. Biol. Chem.* **2020**, *295*, 18316−18327.
(26) Forlani, G.; Sabbioni, G.; Ragno, D.; Petrollino, D.; Borgatti, M. Phenyl-substituted aminomethylene-bisphosphonates inhibit human P5C reductase and show antiproliferative activity against proline-hyperproducing tumour cells. *J. Enzyme Inhib. Med. Chem.* **2021**, *36*, 1248−1257.
(27) Westbrook, R. L.; Bridges, E.; Roberts, J.; Escribano-Gonzalez, C.; Eales, K. L.; Vettore, L. A.; Walker, P. D.; Vera-Siguenza, E.; Rana, H.; Cuozzo, F.; et al. Proline synthesis through PYCR1 is required to support cancer cell proliferation and survival in oxygen-limiting conditions. *Cell Rep.* **2022**, *38*, No. 110320.
(28) Xu, Y.; Zuo, W.; Wang, X.; Zhang, Q.; Gan, X.; Tan, N.; Jia, W.; Liu, J.; Li, Z.; Zhou, B.; et al. Deciphering the effects of PYCR1 on cell function and its associated mechanism in hepatocellular carcinoma. *Int. J. Biol. Sci.* **2021**, *17*, 2223−2239.
(29) Guo, L.; Cui, C.; Zhang, K.; Wang, J.; Wang, Y.; Lu, Y.; Chen, K.; Yuan, J.; Xiao, G.; Tang, B.; et al. Kindlin-2 links mechano-environment to proline synthesis and tumor growth. *Nat. Commun.* **2019**, *10*, No. 845.
(30) Guo, L.; Cui, C.; Wang, J.; Yuan, J.; Yang, Q.; Zhang, P.; Su, W.; Bao, R.; Ran, J.; Wu, C. PINCH-1 regulates mitochondrial dynamics to promote proline synthesis and tumor growth. *Nat. Commun.* **2020**, *11*, No. 4913.
(31) Togashi, Y.; Arao, T.; Kato, H.; Matsumoto, K.; Terashima, M.; Hayashi, H.; de Velasco, M. A.; Fujita, Y.; Kimura, H.; Yasuda, T.; et al. Frequent amplification of ORAOV1 gene in esophageal squamous cell cancer promotes an aggressive phenotype via proline metabolism and ROS production. *Oncotarget* **2014**, *5*, 2962−2973.
(32) Yan, K.; Xu, X.; Wu, T.; Li, J.; Cao, G.; Li, Y.; Ji, Z. Knockdown of PYCR1 inhibits proliferation, drug resistance and EMT in colorectal cancer cells by regulating STAT3-Mediated p38 MAPK and NF-kappaB signalling pathway. *Biochem. Biophys. Res. Commun.* **2019**, *520*, 486−491.
(33) Kuo, C. L.; Chou, H. Y.; Chiu, Y. C.; Cheng, A. N.; Fan, C. C.; Chang, Y. N.; Chen, C. H.; Jiang, S. S.; Chen, N. J.; Lee, A. Y. Mitochondrial oxidative stress by Lon-PYCR1 maintains an immunosuppressive tumor microenvironment that promotes cancer progression and metastasis. *Cancer Lett.* **2020**, *474*, 138−150.
(34) Chen, S.; Yang, X.; Yu, M.; Wang, Z.; Liu, B.; Liu, M.; Liu, L.; Ren, M.; Qi, H.; Zou, J.; et al. SIRT3 regulates cancer cell proliferation through deacetylation of PYCR1 in proline metabolism. *Neoplasia* **2019**, *21*, 665−675.
(35) Kuo, M. L.; Lee, M. B.; Tang, M.; den Besten, W.; Hu, S.; Sweredoski, M. J.; Hess, S.; Chou, C. M.; Changou, C. A.; Su, M.; et al. PYCR1 and PYCR2 Interact and Collaborate with RRM2B to Protect Cells from Overt Oxidative Stress. *Sci. Rep.* **2016**, *6*, No. 18846.
(36) Escande-Beillard, N.; Loh, A.; Saleem, S. N.; Kanata, K.; Hashimoto, Y.; Altunoglu, U.; Metoska, A.; Grandjean, J.; Ng, F. M.; Pomp, O.; et al. Loss of PYCR2 Causes Neurodegeneration by Increasing Cerebral Glycine Levels via SHMT2. *Neuron* **2020**, *107*, 82−94.e86.
(37) Hollinshead, K. E. R.; Munford, H.; Eales, K. L.; Bardella, C.; Li, C.; Escribano-Gonzalez, C.; Thakker, A.; Nonnenmacher, Y.; Kluckova, K.; Jeeves, M.; et al. Oncogenic IDH1 Mutations Promote Enhanced Proline Synthesis through PYCR1 to Support the Maintenance of Mitochondrial Redox Homeostasis. *Cell Rep.* **2018**, *22*, 3107−3114.
(38) Fidalgo, F.; Torrezan, G. T.; Sa, B. C. S.; Barros, B. D. F.; Moredo, L. F.; Valieris, R.; de Souza, S. J.; Duprat, J. P.; Krepischi, A. C. V.; Carraro, D. M. Family-based whole-exome sequencing identifies rare variants potentially related to cutaneous melanoma predisposition in Brazilian melanoma-prone families. *PLoS One* **2022**, *17*, No. e0262419.
(39) Serman, N.; Vranic, S.; Glibo, M.; Serman, L.; Bukvic Mokos, Z. Genetic risk factors in melanoma etiopathogenesis and the role of genetic counseling: A concise review. *Bosnian J. Basic Med. Sci.* **2022**, *22*, 673−682.
(40) Patel, S. M.; Seravalli, J.; Liang, X.; Tanner, J. J.; Becker, D. F. Disease variants of human Delta(1)-pyrroline-5-carboxylate reductase 2 (PYCR2). *Arch. Biochem. Biophys.* **2021**, *703*, No. 108852.
(41) Williams, I.; Frank, L. Improved chemical synthesis and enzymatic assay of delta-1-pyrroline-5-carboxylic acid. *Anal. Biochem.* **1975**, *64*, 85−97.
(42) Forlani, G.; Sabbioni, G.; Ruszkowski, M. Functional Characterization of *Saccharomyces cerevisiae* P5C Reductase, the Enzyme at the Converging Point of Proline and Arginine Metabolism. *Microorganisms* **2022**, *10*, No. 2077.
(43) Yang, Y.; Sauve, A. A. NAD(+) metabolism: Bioenergetics, signaling and manipulation for therapy. *Biochim. Biophys. Acta, Proteins Proteomics* **2016**, *1864*, 1787−1800.
(44) Cambronne, X. A.; Stewart, M. L.; Kim, D.; Jones-Brunette, A. M.; Morgan, R. K.; Farrens, D. L.; Cohen, M. S.; Goodman, R. H. Biosensor reveals multiple sources for mitochondrial NAD(+). *Science* **2016**, *352*, 1474−1477.
(45) Tao, R.; Zhao, Y.; Chu, H.; Wang, A.; Zhu, J.; Chen, X.; Zou, Y.; Shi, M.; Liu, R.; Su, N.; et al. Genetically encoded fluorescent sensors reveal dynamic regulation of NADPH metabolism. *Nat. Methods* **2017**, *14*, 720−728.
(46) Schuck, P. Size-distribution analysis of macromolecules by sedimentation velocity ultracentrifugation and lamm equation modeling. *Biophys. J.* **2000**, *78*, 1606−1619.

https://doi.org/10.1021/acsomega.2c07788
ACS Omega 2023, 8, 3509−3519

(47) Kabsch, W. Xds. *Acta Crystallogr., Sect. D: Struct. Biol.* **2010**, *66*, 125−132.
(48) Evans, P. R. An introduction to data reduction: space-group determination, scaling and intensity statistics. *Acta Crystallogr., Sect. D: Struct. Biol.* **2011**, *67*, 282−292.
(49) Emsley, P.; Lohkamp, B.; Scott, W. G.; Cowtan, K. Features and development of Coot. *Acta Crystallogr., Sect. D: Struct. Biol.* **2010**, *66*, 486−501.
(50) Afonine, P. V.; Grosse-Kunstleve, R. W.; Echols, N.; Headd, J. J.; Moriarty, N. W.; Mustyakimov, M.; Terwilliger, T. C.; Urzhumtsev, A.; Zwart, P. H.; Adams, P. D. Towards automated crystallographic structure refinement with phenix.refine. *Acta Crystallogr., Sect. D: Struct. Biol.* **2012**, *68*, 352−367.
(51) Chen, V. B.; Arendall, W. B., 3rd; Headd, J. J.; Keedy, D. A.; Immormino, R. M.; Kapral, G. J.; Murray, L. W.; Richardson, J. S.; Richardson, D. C. MolProbity: all-atom structure validation for macromolecular crystallography. *Acta Crystallogr., Sect. D: Struct. Biol.* **2010**, *66*, 12−21.
(52) Gore, S.; Sanz Garcia, E.; Hendrickx, P. M. S.; Gutmanas, A.; Westbrook, J. D.; Yang, H.; Feng, Z.; Baskaran, K.; Berrisford, J. M.; Hudson, B. P.; et al. Validation of Structures in the Protein Data Bank. *Structure* **2017**, *25*, 1916−1927.
(53) Liebschner, D.; Afonine, P. V.; Moriarty, N. W.; Poon, B. K.; Sobolev, O. V.; Terwilliger, T. C.; Adams, P. D. Polder maps: improving OMIT maps by excluding bulk solvent. *Acta Crystallogr., Sect. D: Struct. Biol.* **2017**, *73*, 148−157.

https://doi.org/10.1021/acsomega.2c07788
ACS Omega 2023, 8, 3509−3519